Streaming potential of a sand column in partial saturation conditions

Xavier Guichet
École Normale Supérieure, Laboratoire de Géologie, Paris, France
Laboratoire des Géomatériaux, I.P.G.P., Université Paris (Denis Diderot), Paris, France

Laurence Jouniaux
École Normale Supérieure, Laboratoire de Géologie, Paris, France

Jean-Pierre Pozzi
École Normale Supérieure, Laboratoire de Géologie, Paris, France

Received 8 October 2001; revised 1 October 2002; accepted 31 October 2002; published 8 March 2003.

[1] The understanding of the streaming potential in partial water saturation conditions in porous media is of great interest for the interpretation of spontaneous polarization observations. We built a device which allows us to quantify the streaming potential at various saturation conditions using a sand column of 1-m height and 8-cm diameter. This is the first time that such a quantification has been performed. Different gases such as argon, nitrogen, and carbon dioxide are injected into the sand to decrease its water saturation, and to make the fluid flow within the sand. The measured electrokinetic coupling coefficient in partial saturation is either constant or decreases by a factor $\sim$3 with decreasing water saturation from 100 to 40%, whereas the sand electrical resistivity is enhanced by a factor of $\sim$5. *INDEX TERMS:* 5109 Physical Properties of Rocks: Magnetic and electrical properties; 5139 Physical Properties of Rocks: Transport properties; *KEYWORDS:* Streaming potential, partial saturation, electrokinetic, spontaneous potential, transport properties, porous media

Citation: Guichet, X., L. Jouniaux, and J.-P. Pozzi, Streaming potential of a sand column in partial saturation conditions, *J. Geophys. Res.*, *108*(B3), 2141, doi:10.1029/2001JB001517, 2003.

1. Introduction

[2] Spontaneous polarization (SP) anomalies are observed in several geophysical contexts. In tectonically active areas, the timescale of observed SP anomalies prior to earthquakes ranges from a few minutes to a few hours with an amplitude around 100 mV [for a review, see *Park et al.*, 1993]. On volcanoes, SP anomalies are used to define the lateral extent of the hydrothermal zone [*Finizola et al.*, 2002; *Ishido et al.*, 1997; *Jackson and Kauahikaua*, 1987; *Lénat et al.*, 2000; *Malengreau et al.*, 1994; *Zlotnicki et al.*, 1998, 1994] and show usually dipolar characteristics which can reach 4 V [*Finizola et al.*, 1998]. The thermoelectric effect, piezoelectric effect, or electrochemical effect have been proposed to explain SP anomalies, but the best candidate is the streaming potential, i.e., SP created by the motion of an electrolyte through a porous medium, related to a pressure gradient [*Zablocki*, 1978; *Zohdy et al.*, 1973]. Minerals forming the rock develop an electric double layer when in contact with an electrolyte, because the mineral surface is usually negatively charged. Qualitatively the fluid motion drags the electrical double layer with it, and a macroscopic separation of ions appears in the fluid, as the result of convection currents. The macroscopic electrical potential difference ΔV is called the streaming potential.

0148-0227/03/2001JB001517$09.00

[3] In tectonically active zones, SP anomalies could be explained by a mechanism based on the fluid motions between reservoirs triggered by strain perturbations [*Bernard*, 1992], or by changes in high pore pressure in fault zones [*Fenoglio et al.*, 1995]. On volcanoes, the qualitative interpretation is that the negative anomalies observed on the flanks of volcanoes are associated with rainfall, which percolates downward. These negative anomalies can be related to the depth of the water table [*Aubert et al.*, 1993; *Zablocki*, 1978]. The positive anomalies observed on the active zone have their origin in upward convective flows [*Aubert and Kieffer*, 1984; *Zablocki*, 1978], and are used to define the hydrothermal zone. Electroseismic investigations are also based on the electrokinetic phenomena and are used to detect small rock interface property changes like permeability and saturation state [*Beamish*, 1999; *Garambois and Dietrich*, 2001].

[4] Modeling of all these observations needs a good understanding of electrokinetic phenomena. Therefore experimental studies have been performed for a better understanding of the electrokinetic effect at the level of the rock-electrolyte interface. Many streaming potential measurements have been made on crushed rocks at various temperatures or pH [*Ishido and Mizutani*, 1981; *Lorne et al.*, 1999a], on rock samples [*Jouniaux et al.*, 2000; *Jouniaux and Pozzi*, 1995, 1997; *Pengra et al.*, 1999], and during deformation [*Jouniaux et al.*, 1994; *Jouniaux and Pozzi*, 1995; *Lorne et al.*, 1999b; *Yoshida*, 2001]. However,

only a few experiments have studied streaming potentials in two-phase flow conditions. *Antraygues and Aubert* [1993] measured the electrokinetic potential generated by wet steam flow in a vertical cylindrical column of porous material, using nonpolarising electrodes. They observed that the potential is mainly a function of the vapor flow rate, and an increase in the fraction of vapor can induce a large and long-lived increase in the potential differences along the vapor flow direction. Two-phase flow observations [*Antraygues and Aubert*, 1993; *Jiang et al.*, 1998; *Sprunt et al.*, 1994] are in agreement with the fact that partial saturation should increase the streaming potential, with or without a temperature effect, because the electrical resistance of the medium is increased.

[5] Measurements of streaming potentials of partially saturated rocks are therefore crucially needed since the partially saturated zone has to be taken into account to model and to interpret the SP observations. Indeed understanding and monitoring the distribution and transport of water using SP measurements has recently been reinvestigated [*Gibert and Pessel*, 2001; *Ishido and Pritchett*, 1999; *Sailhac and Marquis*, 2001]. Moreover, *Bernard* [1992] reported that strong local amplification was required for a streaming potential to be observed at long distances from its source. The effect of nonsaturating conditions on the streaming potential is expected to largely enhance the electrical signal, related to an enhancement of the electrical resistivity of the medium, and thus to be of great interest in the interpretation of SP observations. Nevertheless to take into account the electrokinetic coupling in partially saturated zones, geophysical methods must rely on accurate laboratory measurements for calibration.

[6] Measurements of streaming potential as a function of water saturation have not previously been reported in the literature. In this paper we measure the streaming potential in a column of sand in two-phase flow conditions, at various water saturations. Of specific interest to this study is the form and the magnitude of the coupling coefficient when the water content of the porous medium changes. Our measurements are the first quantification of the evolution of the electrokinetic coupling coefficient as a function of the water saturation. Attempts to model streaming potential in partial saturation state are also scarce, and hence we propound a phenomenological law describing the behavior of the coupling coefficient as a function of water saturation. Our measurements have also been compared to the model recently derived by *Revil et al.* [1999b].

2. Electrokinetic Phenomena

[7] In a saturated porous medium, and steady-state fluid circulation, a linear relation is observed between the macroscopic electrical potential difference ΔV and the applied pressure difference ΔP. The ratio $\Delta V/\Delta P$ is called the electrokinetic coupling coefficient (V/Pa):

$$C_{\mathrm{HS}} = \Delta V/\Delta P = (\varepsilon\zeta)/(\eta\sigma_f), \tag{1}$$

where ζ is the zeta potential defined as the electric potential on the shear plane, σ_f is the electric conductivity of the circulating fluid, $\varepsilon = \varepsilon_{\mathrm{water}}\,\varepsilon_0$ is the electric permittivity of the fluid with $\varepsilon_{\mathrm{water}}$ the relative dielectric constant of the fluid and $\varepsilon_0 = 8.84 \times 10^{-12}$ F/m the dielectric constant of vacuum, and $\eta = 10^{-3}$ Pa.s is the shear viscosity of the circulating fluid. The relative permittivity of water used is computed as a function of temperature according to results of *Malmberg and Maryott* [1956]. Equation (1) is obtained with the Helmholtz-Smoluchowski model, and it implies that the surface conductivity is small and negligible compared to the fluid conductivity σ_f, and that the convection and back currents are of equal magnitude and opposite along the same path [*Dukhin and Derjaguin*, 1974].

[8] Several models take into account the effects of surface electrical conductivity σ_s. For example, an empirical correction [*Ishido and Mizutani*, 1981; *Jouniaux et al.*, 2000; *Lorne et al.*, 1999a] replaces the electrolyte conductivity σ_f by the effective conductivity σ_{eff} in equation (1); the effective conductivity is defined by

$$\sigma_{eff} = F\sigma_r \tag{2}$$

where F is the formation factor and σ_r the electrical conductivity of the rock when the rock is saturated by a fluid, which has the same electrical conductivity than the fluid used for the electrokinetic measurement, and including possible surface conductivity.

[9] For a complete development of the equations governing the coupled electro-magnetics and flow of porous media, see *Pride* [1994], and *Revil et al.* [1999a, 1999b], and for further details on surface conductivity, see *Glover et al.* [1994] and *Revil and Glover* [1998].

[10] The effects of partial saturation S_w are not taken into account in equation (1). Recently *Revil et al.* [1999b] derived a new equation, which relates the electrokinetic coupling coefficient to the partial water saturation. The equation derived by *Revil et al.* [1999b] is rigorously valid for $m = n = 2$, with m being the Archie's first exponent ($m = -\ln F/\ln \Phi$ where Φ is the porosity) and n is Archie's second exponent ($\sigma_r(S_w < 1) = \sigma_r(S_w = 1)\, S_w^n$ where S_w is the water saturation) [*Archie*, 1942]. In the high-salinity domain (i.e., $\sigma_f \geq 5\ (m-1)\sigma_s$), following the calculation process of *Revil et al.* [1999b] coupling results of Bussian's model [*Bussian*, 1983] with results of the model of *Pride* [1994], we have generalized their results to any values of m and n:

$$C(S_e \leq 1) = \frac{\varepsilon\zeta/\eta\sigma_f}{S_e^n\left(1 + m\left(\frac{F}{S_e^n} - 1\right)\frac{(\sigma_s/\sigma_f)}{S_e}\right)} \tag{3}$$

where S_e is the effective water saturation defined by

$$S_e = \begin{cases} \dfrac{S_w - S_{w0}}{1 - S_{w0}} & \text{as} \quad S_e > S_{w0} \\ 0 & \text{as} \quad S_e < S_{w0} \end{cases}. \tag{4}$$

where S_w is the water saturation and S_{w0} the water saturation below which there is no longer flow of the wetting phase. *Revil et al.* [1999b] foresaw an enhancement of the streaming potential with a decrease in the water saturation from unity to a critical value

$$S_e^c = \left(F\frac{\sigma_s}{\sigma_f}\right)^{1/(n+1)} \tag{5}$$

and that the coupling coefficient decreases below this critical value with decreasing water saturation until the S_{w0} water saturation value is reached.

[11] To take into account the influence of the partial saturation in equation (3), *Revil et al.* [1999b] used an equation for the electrical conductivity in partial saturation, which reduces in the high salinity domain to

$$\sigma_r = \frac{\sigma_f}{F} S_e^n + m\left(1 - \frac{S_e^n}{F}\right)\frac{\sigma_s}{S_e} \tag{6}$$

This equation is obtained using empirical relationships developed by *Archie* [1942] and *Waxman and Smits* [1968]. However, equation (6) fails to explain the evolution of the electrical conductivity of a rock/fluid mixture below the critical water saturation S_e^c, since according to equation (6) the electrical conductivity of a rock/fluid mixture is expected to increase below the critical water saturation until the effective water saturation goes to zero. The increase of the electrical conductivity of a rock/fluid mixture with decreasing saturation has no physical meaning, since gas bubbles in the porous space behave like insulators. Therefore equation (3) can be only compared to measurements when the effective water saturation is greater than S_e^c.

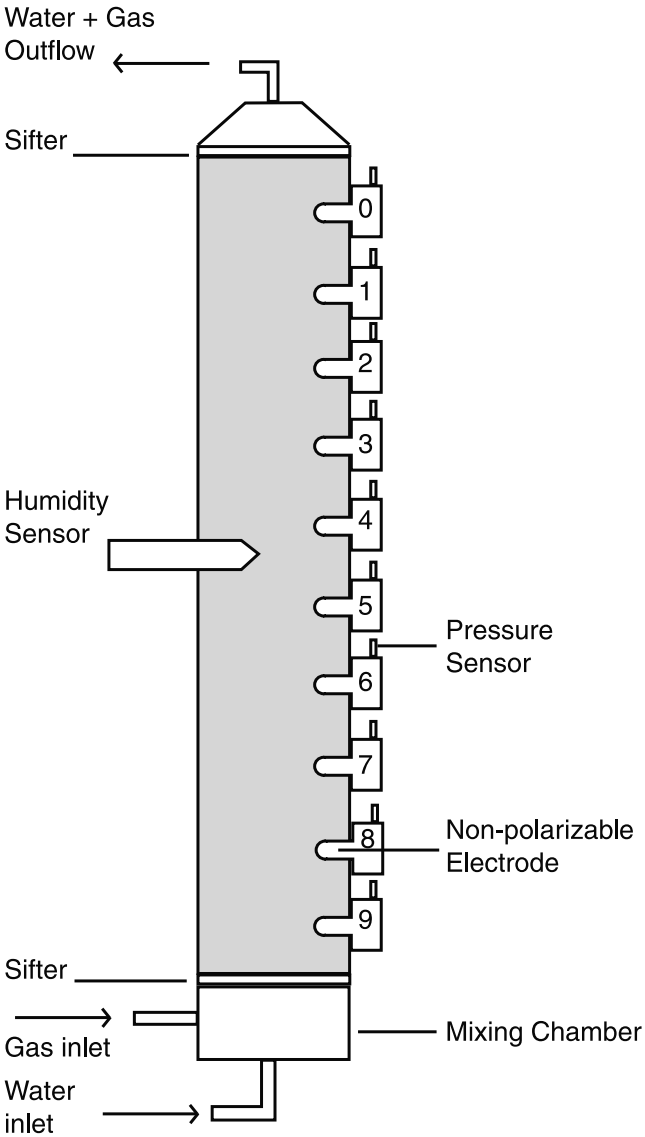

Figure 1. Sketch of the sand column of 1-m height and 8-cm diameter. Ten pressure sensors and electrodes are located along the column every 10 cm.

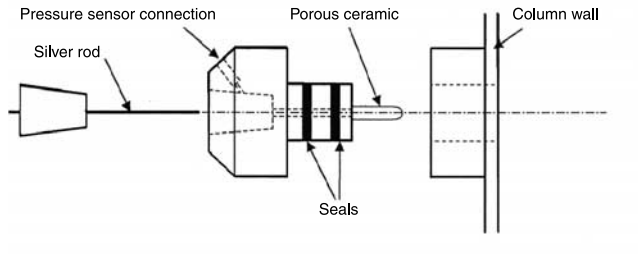

Figure 2. Sketch of an electrode.

[12] Equation (3) takes into account only the enhancement of the electrical potential caused by the insulating role of gas bubbles. In fact, the effects of gas bubbles in the pore are more complicated. There is a ζ-potential at the liquid-gas interface [*Graciaa et al.*, 1995]; the gas can react with the solution and change pH, and conductivity. These changes can be monitored but new ionic species due to gas dissolution can be adsorbed onto the mineral surface and can change the ζ-potential. The modification of the species adsorbed is not easy to take into account, and the reactions are not always known so that it is not possible to quantify a change in the ζ-potential.

3. Experimental Apparatus

[13] We use a 1-m high cylindrical column with an 8 cm inside diameter (Figure 1) that we fill with sand of known petrophysical properties. The water is made to flow through the sand column from bottom to top, using a reservoir located at incremental heights. Along the column, an electrode and a pressure sensor are placed every 10 cm. We monitor the humidity in the middle of the column by a capacitive sensor. At each end of the column sifters with 30 μm meshes allow measurement of the electrical resistivity of the whole column by an HP 4284A impedancemeter.

[14] We acquired the data in differential mode using high-resistance amplifiers and silver-silver chloride nonpolarising electrodes (Figure 2). They are grounded by coaxial wire, earthed at one of the 10 electrodes, which are numbered 0–9 from the top of the column (Figure 1). Each rod is put into a porous ceramic pot filled with deionised water, which is in contact with the porous medium, so that charge accumulation on the rods is avoided. The porous ceramics remain saturated unless a pressure of 0.1 MPa is applied, and therefore remain electrically conducting.

[15] Electrical surface conductivity is determined following the process drawn up by *Waxman and Smits* [1968]. A small device formed by a PVC cylinder 2.5 cm in diameter and 10 cm long, filled with the sand under study, enables us to measure the electrical conductivity of the sand for several electrolyte conductivities. Each measurement is made after waiting 1 day to ensure equilibrium between the electrolyte

Table 1. Measured Petrophysical Properties of the Sand[a]

Experiments	F	σ_s, S/m	n	Permeability, m^2
1–29	22	$<10^{-4}$	1.3	3×10^{-12}
30–43	15	$<10^{-4}$	1.3	3×10^{-12}

[a]F, formation factor; σ_s, electrical surface conductivity; n, Archie's second exponent.

and sand. We add sodium chloride in distilled water to control the conductivity of the electrolytes.

4. Method of Measurements

[16] The sand is sifted to have a mean grain diameter of 300 μm. In order to determine the initial mineralogy of the sand and possible mineralogical changes, we carry out X-ray diffraction analyses before any fluid circulation and after the circulation of each kind of gas.

[17] Once the column is filled with sand, we perform all the experiments for one kind of gas (argon or nitrogen), at various states of saturation. We only empty and refill the column with the same sand when we test a new gas.

[18] Deionised water is forced through the sand to saturate the pore space. The liquid-phase saturation S_w is measured with the capacitive sensor. First we check the linearity between fluid flow and pressure gradient for several heights of the water reservoir, and we calculate the permeability of the column using Darcy's law. Second a water reservoir height is chosen, and we check the linearity between the electrical potential gradient and the pressure gradient, leading to the saturated state coupling coefficient $C_m(S_w = 1)$.

[19] Then the reservoir is disconnected from the column. Gas is forced through the sand with a constant pressure of injection. The inlet pressure ranges from 29 to 32 kPa for argon injections, and from 23 to 30 kPa for nitrogen injections. The motion of the gas bubbles induces fluid flow, since gas circulation empties water from the column. Gas injection is maintained as long as necessary to reach a steady state, which is determined by the constant water flow rate. Flow rate values are around 10^{-3} l per min. Measurements of electrical potential and pressure of the steady state allow us to obtain an electrokinetic coefficient, for a partially saturated state $C_m(S_w)$. After each experiment, the electrical conductivity of the column is measured at 1 kHz, to determine Archie's second exponent.

[20] After circulation through the column, a sample of water is collected to measure pH and electrical conductivity. The chemical species, which are dissolved by circulation through the sand, are also tested.

5. Experimental Results

5.1. Petrophysical Properties of the Sand Column

[21] Table 1 lists the petrophysical properties of the sand column. X-ray diffraction revealed two kinds of sand minerals: quartz is the major component at around 98%, calcite the remaining 2%. After water circulation and gas injection, either argon or nitrogen, the major changes in composition are a decrease of the calcite peak associated with calcite dissolution. Calcite dissolution is revealed by chemical fluid analysis (Table 2), and the pH of the solutions (Tables 3 and 4) ranges from 6.8 to 8.7. The calcite-water-atmospheric CO_2 system balances at pH about 8.6 at room pressure and temperature [*Sigg et al.*, 2000].

[22] When the sand electrical conductivity is measured as a function of water conductivity, the conductivity of the fluid, which came out off the sand was never less than 4×10^{-3} S/m, even if the sand was saturated with distilled water. The increase of the fluid conductivity is related to exchange of ions between fresh distilled water and the rock matrix. Therefore the electrical surface conductivity of the sand cannot be measured exactly (Figure 3), but is estimated to be smaller than 2×10^{-4} S/m. *Revil and Glover* [1998] reported a surface conductance of 8×10^{-9} S for quartz, independent on the electrolyte conductivity when it exceeds 10^{-2} S/m. Electrical conductivities of the water circulating in the sand column are around 10^{-2} S/m (see Tables 3 and 4), so that we assume that the specific surface conductance of the sand is 8×10^{-9} S which is equivalent to a surface conductivity of about 1.0×10^{-4} S/m for a mean grain diameter of 300 μm. Note that the formation factor observed in Figure 3 is not the formation factor of the sand column; the sand is not packed down as it is in the column.

[23] Archie's second exponent n is deduced to be 1.3 according to equation (6) with negligible surface conductivity, by measuring the sand conductivity for several water saturations (Figure 4). *Waxman and Smits* [1968] reported that the n value is close to the value of Archie's first exponent m. *Archie* [1942] measured m of about 1.3 for relatively coarse granular media, giving confidence in the value of n that we deduced. The measured normalized

Table 2. Chemical Analyses of the Solutions After Flowing Through the Sand[a]

Experiment	Gas	Na^+, 10^{-3} mol/l	K^+, 10^{-3} mol/l	Ca^{2+}, 10^{-3} mol/l	Mg^{2+}, 10^{-3} mol/l	Cl^-, 10^{-3} mol/l	SO_4^{2-}, 10^{-3} mol/l	HCO_3^-, 10^{-3} mol/l	SiO_2, 10^{-3} mol/l	NH_4^+, 10^{-3} mol/l
1	none	0.191	0.095	0.719	0.010	0.257	0.036	1.515	0.218	···
18	argon	0.191	0.097	0.489	0.006	0.195	0.021	1.030	0.175	···
19–22	argon	0.213	0.097	0.559	0.005	0.186	0.065	1.394	0.184	···
23–25	argon	0.183	0.077	0.499	0.004	0.171	···	1.233	0.170	···
26–27	argon	0.178	0.072	0.584	0.003	0.210	0.021	1.313	0.166	···
33	nitrogen	0.161	0.036	0.514	0.019	0.149	···	1.010	0.180	0.025
34	nitrogen	0.174	0.059	0.599	0.016	0.171	···	0.909	0.161	0.026
35	nitrogen	0.148	0.056	0.367	0.009	0.460	···	···	0.082	0.010
39	nitrogen	0.148	0.026	0.302	0.007	0.282	0.052	0.534	0.170	0.017
41	nitrogen	0.157	0.023	0.402	0.009	0.138	···	1.010	0.184	0.027

[a]Amount of ion was not measured.

Table 3. Measurements of Coupling Coefficient $C_m(S_w \leq 1)$[a]

Experiment	Temperature, °C	Fluid Conductivity, μS/cm	pH	Saturation, S_w	C_m, mV/MPa	Error,%	Zeta Potential, mV	
							By equation (1)	By equation (8)
1	25.3	178	7.3	1	−1140	8	−29	···
2	20	99	8.0	1	−1750	5	−24	···
3	20.6	98	8.1	1	−1710	3	−24	···
4	19.8	93.5	8.0	1	−1780	1	−23	···
5	20.4	89.5	8.5	1	−1430	10	−18	···
6	21	91	8.4	1	−1660	4	−21	···
7	19.8	90.5	8.3	1	−1720	3	−22	···
8	20.4	90.5	8.3	1	−1730	4	−22	···
9	20.6	90	8.4	1	−1550	6	−20	···
10	20.8	102	8.7	1	−1660	5	−24	···
11	20.4	106.6	8.4	1	−1720	3	−26	···
12	20.4	105	8.5	1	−1760	2	−26	···
13	20.4	104	8.6	1	−1760	3	−26	···
14	20.6	99.2	8.5	1	−1740	4	−24	···
15	20.6	95.3	8.5	1	−1650	3	−22	···
16	21.3	264	8.1	1	−960	32	−36	···
17	24.6	145	7.9	0.81	−1290	4	−27	−22
18	25	146.8	8.0	0.73	−997	9	−21	−15
19	25	152	8.0	0.66	−866	13	−19	−13
20	24.6	164	8.1	0.65	−916	7	−22	−14
21	24.6	157	8.2	0.58	−1010	2	−23	−13
22	24.6	147	8.3	0.55	−1060	2	−22	−12
23	24.4	139	8.3	0.51	−1100	2	−22	−11
24	22.8	146	8.4	0.52	−721	12	−15	−8
25	23	133	8.5	0.48	−732	18	−14	−7
26	23.2	126	8.5	0.48	−860	14	−16	−7
27	23.2	126	8.6	0.46	−575	35	−10	−5
28	24.4	115.5	8.7	0.44	−669	30	−11	−5
29	24.4	105.5	8.7	0.43	−843	16	−13	−5

[a]Experiments 1–16 are conducted in saturated conditions and 17–29 are conducted when argon is forced through the sand column, at various water saturation S_w.

electrical resistivity is enhanced by a factor of about 5 while water saturation is decreased from 100 to 40%.

5.2. Coupling Coefficients Measurements

5.2.1. Saturated Sand Column

[24] The electric potential variations induced by pressure variations corresponding to water reservoir height of 0.6 m are shown in Figure 5. All potential measurements are referenced to electrode 0. The cause of the electrical noise with a period of about 60 s is not known. We note that the magnitude of the streaming potential is only about few mV, and measurements of streaming potential below 1 mV are difficult because of the noise. When a plateau is reached for both pressure and electrical potential, the changes in pressure and in potential are calculated from the initial state, for each electrode and pressure sensor couple. The potential varia-

Table 4. Measurements of Coupling Coefficient $C_m(S_c \leq 1)$[a]

Experiment	Temperature, °C	Fluid Conductivity, μS/cm	pH	Saturation, S_W	C_m, mV/MPa	Error, %
30	20	138	6.8	1	−1530	13
31	20	138	6.8	1	−1380	37
32	20	148	8.0	0.74	−2360	63
33	20	130	8.2	0.80	−1620	4
34	20	122	8.0	0.83	−1600	9
35	20	96	8.3	0.48	−1090	12
36	20	96	8.3	0.45	−1380	4
37	20	96	8.3	0.44	−1520	4
38	20	96	8.3	0.41	−1440	5
39	25	91	8.4	0.59	−1520	1
40	25	85	8.3	0.53	−1950	4
41	25.3	102	8.0	0.69	−1720	1
42	25.3	110.5	8.2	0.59	−2440	16
43	27.4	128	7.8	0.66	−1540	2

[a]Experiments 30–31 are conducted in saturated conditions and 32–43 are conducted when nitrogen is forced through the sand column, at various water saturation S_w.

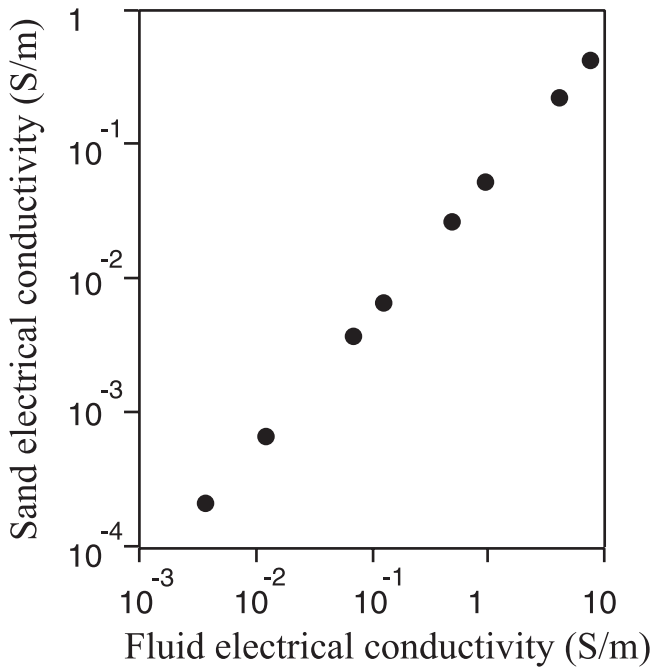

Figure 3. Electrical conductivity of the sand as a function of the electrical conductivity of NaCl solutions.

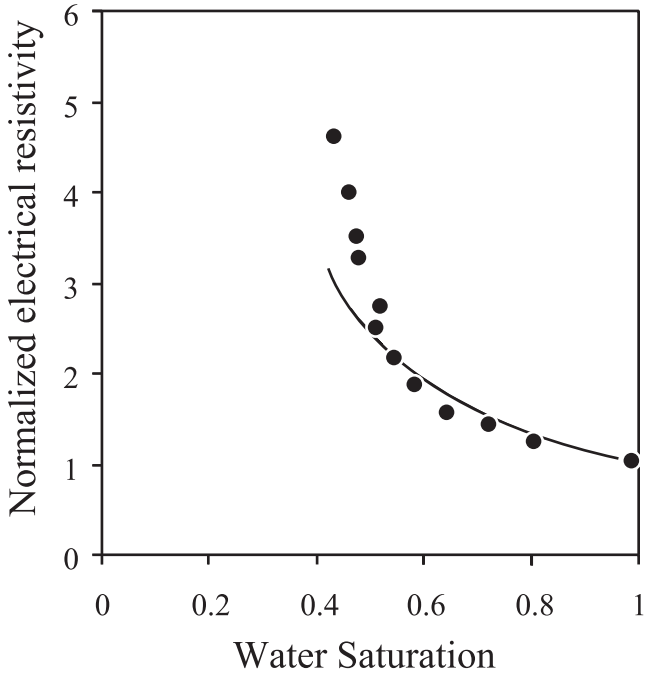

Figure 4. Normalized electrical resistivity of the sand as a function of water saturation. The curve fit to Archie's second law leads to $n = 1.3$.

tions of the eight electrodes as a function of the imposed pressure variation are shown in Figure 6. Linear regression (Figure 6) gives a value of the coupling coefficient: $C_m(S_w = 1) = -1140 \pm 92$ mV/MPa. In this experiment, (experiment 1 in Table 1) $\sigma_f = 1.78 \times 10^{-2}$ S/m, pH = 7.3.

5.2.2. Partially Saturated Sand Column

[25] A first result is that the streaming potential remains proportional to the driving pressure when the sand is not saturated (Figure 7). Measured coupling coefficients at various saturations are shown in Tables 3 and 4 when argon and nitrogen are made to flow respectively.

[26] The measured coupling coefficients range from -575 to -2440 mV/MPa, depending on water saturation, electrical conductivity, and pH of the electrolyte (Tables 3 and 4). The variation of the coupling coefficient versus water saturation is shown in Figure 8 for argon and nitrogen circulation. In the case of argon circulation, a decrease of the coupling coefficient (in absolute value) is observed with decreasing water saturation. While the water saturation varies from 1 to 0.4, the absolute value of the coupling coefficient is reduced by a factor of $\sim$3. The coupling coefficients obtained with nitrogen circulation have large error bars, and it is difficult to distinguish a clear behavior versus water saturation. The coupling coefficient remains roughly constant.

[27] With decreasing water saturation, the electrical conductivity and the pH of the electrolyte also change as shown in Tables 3 and 4. Therefore the variations in coupling coefficients shown in Figure 8 may be also related to electrical conductivity and pH variations.

6. Discussion

[28] We begin by looking for a simple relation between water saturation and the measured coupling coefficients without taking into account changes in water pH and conductivity (Figure 8). In the case of argon circulation, it appears that the coupling coefficient decreases lineary with increasing water saturation:

$$C(S_w \leq 1) = AS_w + B \tag{7}$$

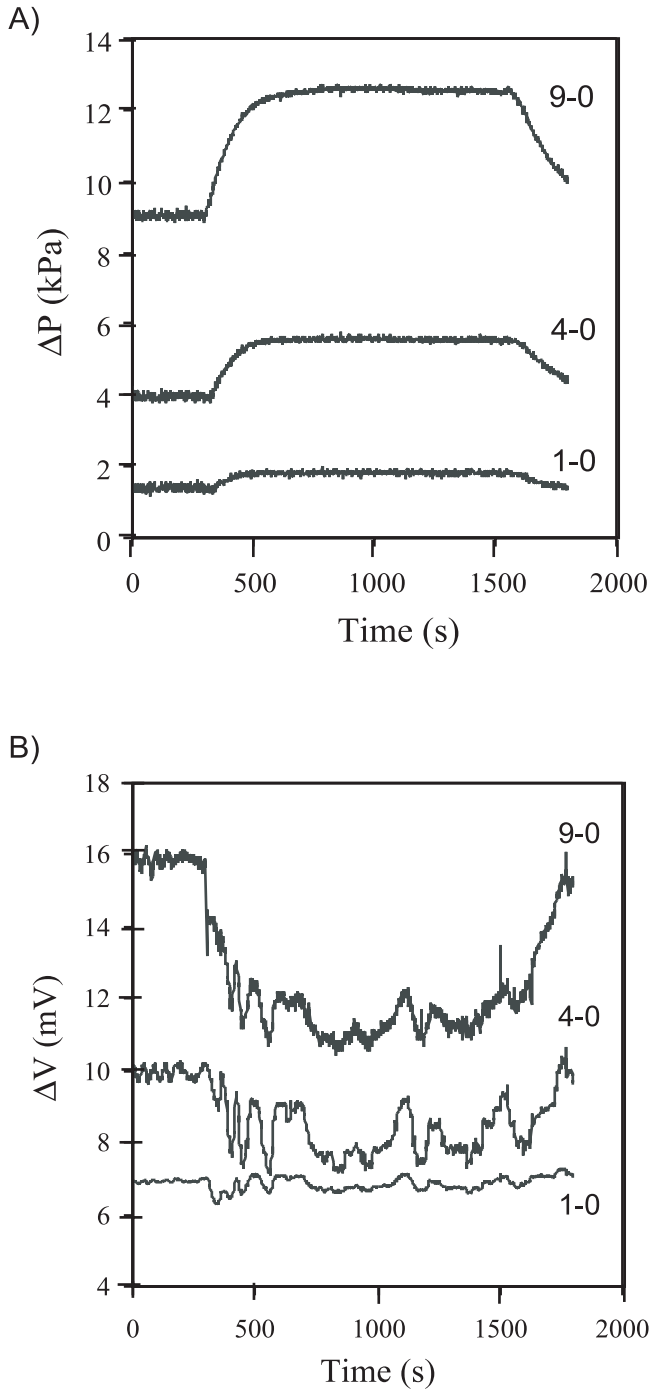

Figure 5. (a) Evolution of three pressure differences referenced to the sensor 0 with the reservoir located at around 60 cm above the top of the column. Water flows between 300 and 1600 s. (b) Evolution of three electrical potential differences referenced to the electrode 0, when water is forced through the sand column with the same conditions as in Figure 5a.

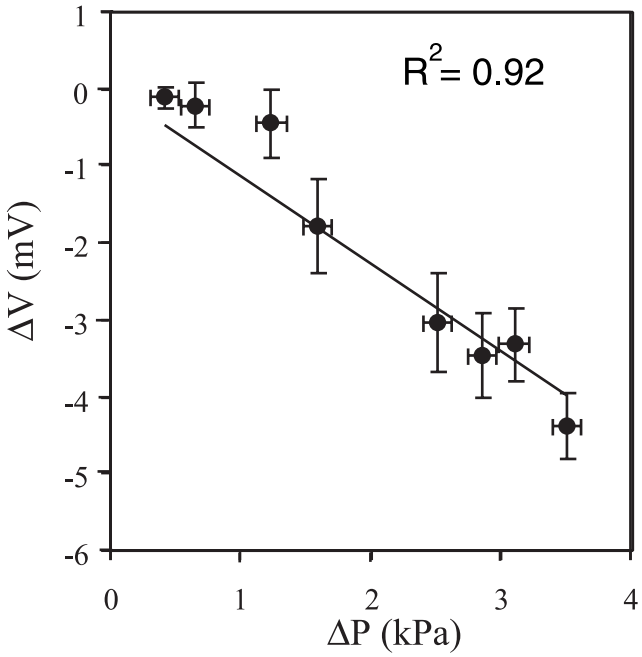

Figure 6. Streaming potential differences versus applied pressure differences in steady state and saturated state. The determination of the coupling coefficient is from the linear regression curve shown.

where A and B are constants. Since there is no fluid flow when the porous medium is totally dry, B should be equal to zero. When the water saturation equals unity, the simplest expression of the constant A is the Helmholtz-Smoluchowski relation (equation (1)). This relation is valid when the surface electrical conductivity of the sample is negligible. Since the surface electrical conductivity for our sample is too low to be measured, we assume that equation (1) is valid. Therefore equation (7) becomes

$$C(S_w \leq 1) = \frac{\varepsilon\zeta}{\eta\sigma_f} S_w \tag{8}$$

We have to take into account the variation of the ζ-potential with fluid conductivity in order to compare our measurements to the coupling coefficient calculated according to

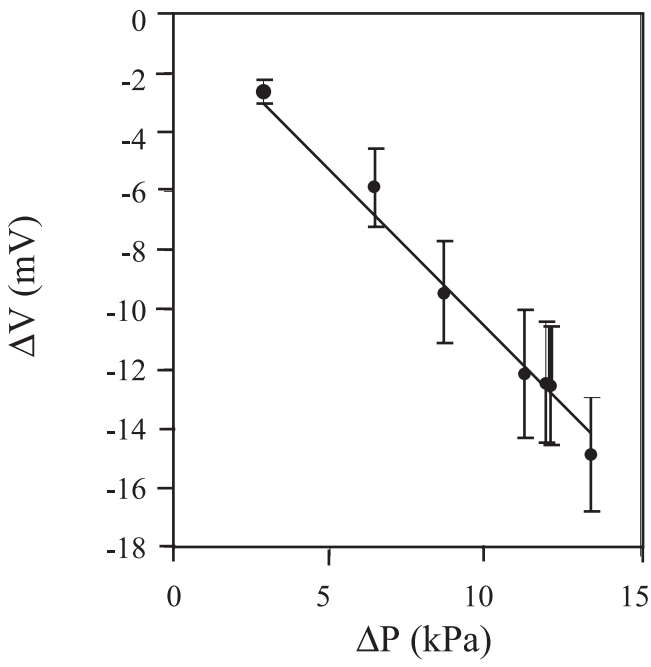

Figure 7. Streaming potential differences versus applied pressure differences in steady state and partially saturated state. The determination of the coupling coefficient is from the linear regression curve shown.

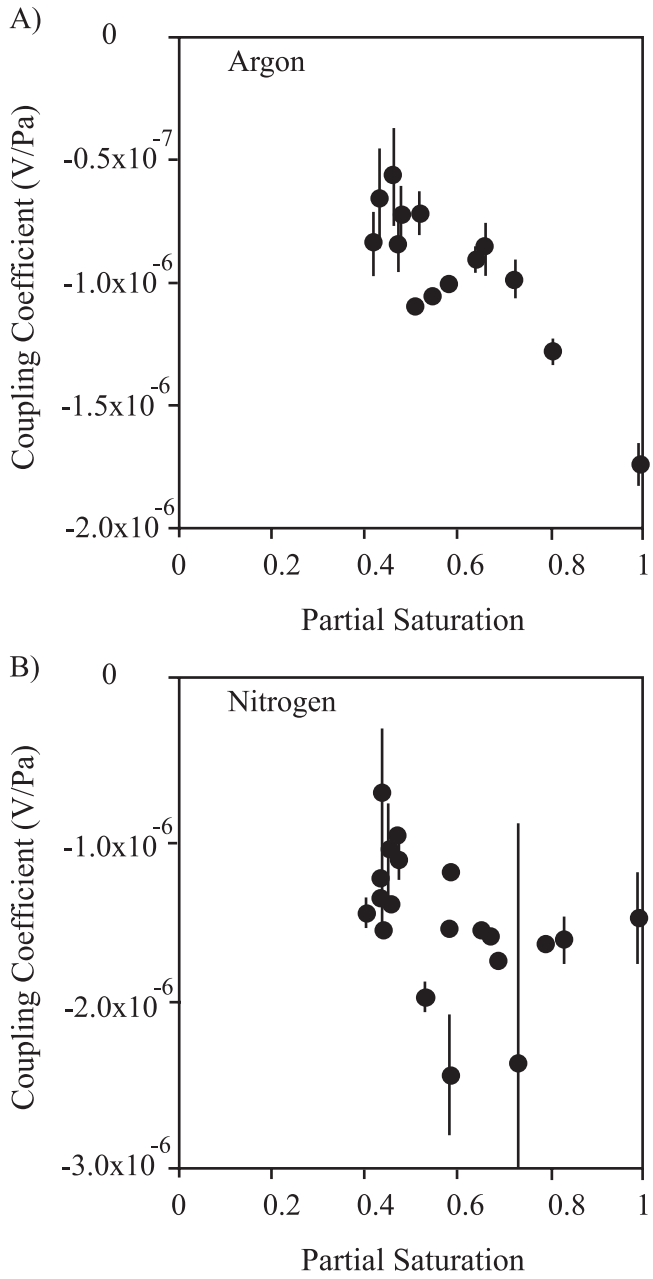

Figure 8. Variation of the measured coupling coefficient versus water saturation. Water pH and conductivity changes are reported in Tables 3 and 4. (a) Argon circulation. (b) Nitrogen circulation.

equation (8). To compute equation (8), all the parameters are measured except the ζ-potential. Since the ζ-potential originates at the water-rock interface and is related to the water composition [*Davis and Kent*, 1990; *Ishido and Mizutani*, 1981], we make the assumption that the ζ-potential is not influenced by the saturation state for our experiments. This assumption can be justified by (1) nitrogen and argon are inert gases which do not change the chemical composition of the circulating water, (2) the liquid phase remains the wetting phase because the water saturation is always greater than 0.4 (Tables 3 and 4). Point (2) is deduced from our electrical resistivity measurements (Figure 4); indeed in water wet systems, the electrical resistivity of rocks shows two domains as a function of water saturation. In the first, the resistivity increase is associated with the removal of bulk water, the normalised resistivity, and the water saturation are linear in a log resitivity-linear saturation plot, and the resistivity increase is about 1 order of magnitude; in the second, the resistivity increase is partly caused by water inside the network which is physically isolated by gas bubbles. The film of water wetting the grain surface provides a path for electrical flow, and the normalised resistivity shows an increase of several orders in magnitude in a log linear plot versus water saturation. The reader can find, for example, measurements of electrical resistivity versus water saturation in the work of *Roberts and Lin* [1997] and simulation in the work of *Suman and Knight* [1997]. In our study, the normalised electrical resistivity is increased only by about ~5 (Figure 4), so that the current path is provided by bulk water, meaning that the electrical double layer is not disturbed by gas bubbles.

[29] Next we seek an empirical expression from which to estimate ζ-potential versus water conductivity to insert into equation (8). Using our measurements performed in saturated state at pH = 8.3 ± 0.25, the ζ-potential according to equation (1) is related to the electrolyte electrical conductivity in the range $10^{-2} - 2.5 \times 10^{-2}$ S/m by a logarithmic relation (Figure 9)

$$\zeta(V) = -0.0146\ln(\sigma_f) - 0.0854 \tag{9}$$

meaning that the ζ-potential decreases with increasing fluid conductivity, which is the reverse of the usual variation. Actually the ζ-potentials measured on crushed Fontainebleau sandstones by *Lorne et al.* [1999a] show an increase, with increasing fluid electrical conductivity, of about 20 mV per decade in the range 10^{-4} to 10^{-1} S/m, in agreement with the compilation of *Pride and Morgan* [1991]

$$\zeta(\mathrm{mV}) \propto 20\log_{10}(\sigma_f) \tag{10}$$

We do not discuss here this unusual variation of ζ-potential with fluid electrical conductivity. Knowing the fluid electrical conductivity for each experiment, the ζ-potential is calculated using equation (9), and the electrokinetic coupling coefficient is computed with equation (8) for various saturation states, and compared to the measured electrokinetic coupling coefficient in Figure 10. In the case of argon circulation, the calculated coupling coefficients are in reasonable agreement with the measured coupling

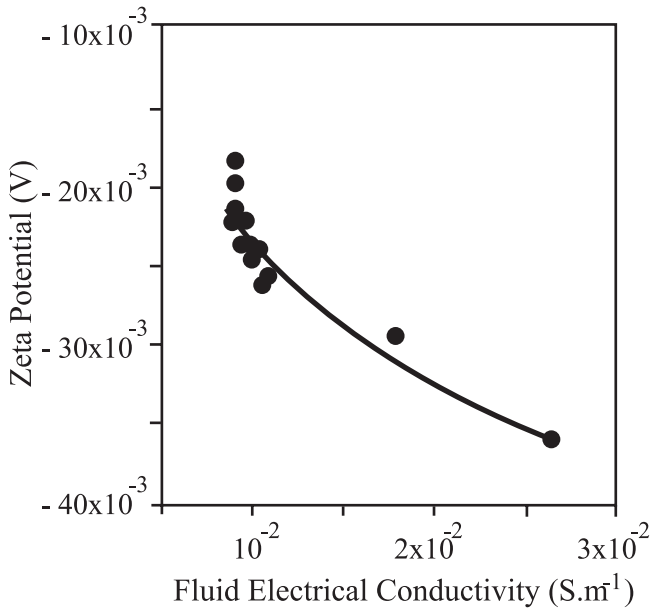

Figure 9. Variation of the ζ-potentials deduced using equation (1) from the measured coupling coefficients in saturated state (experiments 1–16) as a function of the fluid electrical conductivity. The pH values are in the range 7.3–8.7.

coefficients (Figure 10a). On the other hand, equation (8) fails to explain the measurements in the case of nitrogen circulation (Figure 10b). When using equation (10) to describe the variation of zeta potential with water conductivity, the results are roughly the same.

[30] Since a relatively good estimate of the coupling coefficient in partial saturation is obtained in Figure 10a for argon circulation, we compare the ratio $C_m(S_w < 1)/C_m(S_w = 1)$ of the measured coupling coefficient in partial water saturation to the measured coupling coefficient of the saturated sand, with the ratio

$$\frac{C(S_w \le 1)}{C(S_w = 1)} = S_w \tag{11}$$

in order to interpret the evolution of the measured coupling coefficient versus water saturation. To compare the ratio $C_m(S_w < 1)/C_m(S_w = 1)$ to the ratio as in equation (11), experiments in saturated and in partially saturated states must be conducted with the same pH and electrical conductivity of the electrolyte. Otherwise we will not be able to discern the variations of the coupling coefficient related to electrolyte properties from the variations of the coupling coefficient related to the partial saturation condition. The ζ-potential depends on the electrical conductivity and on the pH of the electrolyte, but the partial saturation is not assumed to have an influence on the ζ-potential [*Revil et al.*, 1999b]. Thus the ζ-potential is deduced from our measurements according to equation (8), and empirical relations are used to correct pH and fluid electrical conductivity variations. To perform pH corrections, we use the experimental law determined by *Lorne et al.* [1999a] for crushed Fontainebleau sandstones, which relates the ζ -

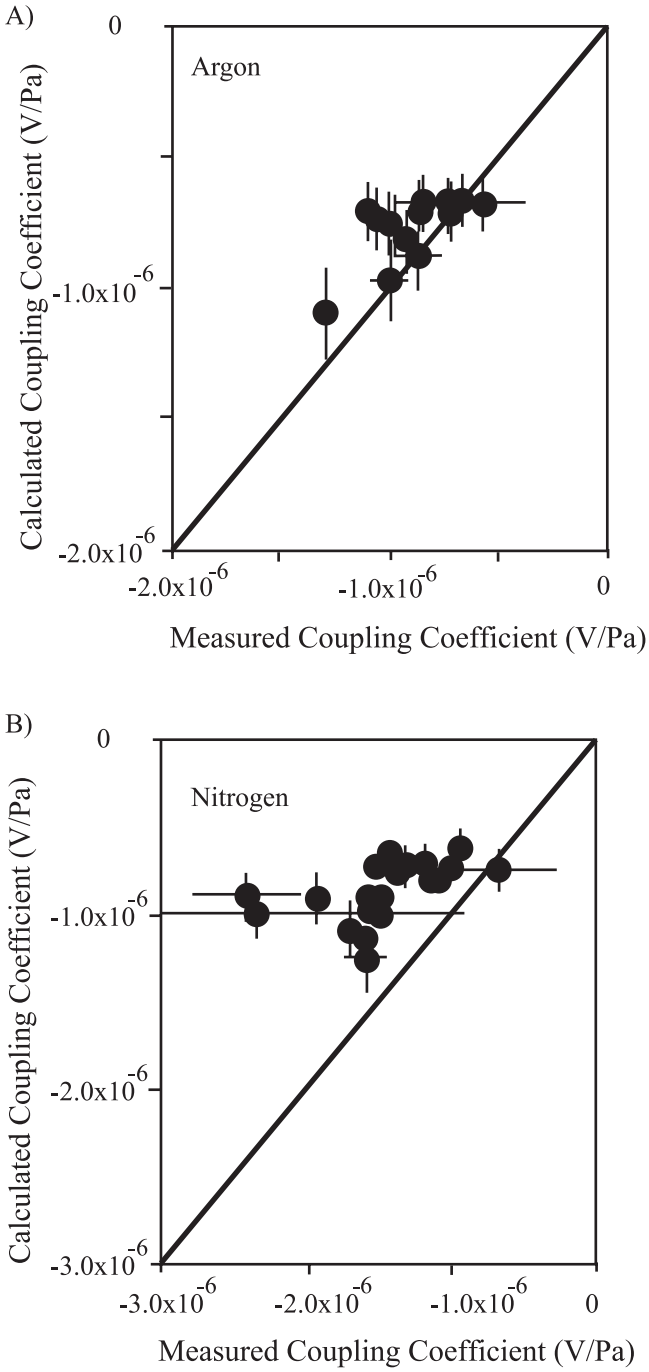

Figure 10. Coupling coefficient in partial saturation state. Comparison between the prediction of the coupling coefficient from equation (8) using equation (9) to calculate the ζ-potential and our measurements. The line has a slope of unity to compare measured and calculated values.

potential (in V) measured at pH = pH_0 to the ζ-potential at pH = pH_1 through a linear relation

$$\zeta(pH_1) = (pH_0) - (pH_1 - pH_0) \times 1.45 \times 10^{-3} \qquad (12)$$

[31] Electrolyte conductivity corrections are made using either equation (9) or equation (10). The ratio C_m ($S_w < 1$)/$C_m(S_w = 1)$ that would have been measured at a fixed pH (pH = 8) and a fixed fluid electrical conductivity (1.4×10^{-2}) is calculated using the corrected ζ-potential values in accordance with equation (13)

$$\frac{C_m(S_w \le 1)}{C_m(S_w = 1)} = \frac{\zeta(S_w \le 1)}{\zeta(S_w = 1)} \times S_w \qquad (13)$$

[32] When argon is made to flow, the saturation ranges from approximately 40 to 80% (Figure 11). The normalized

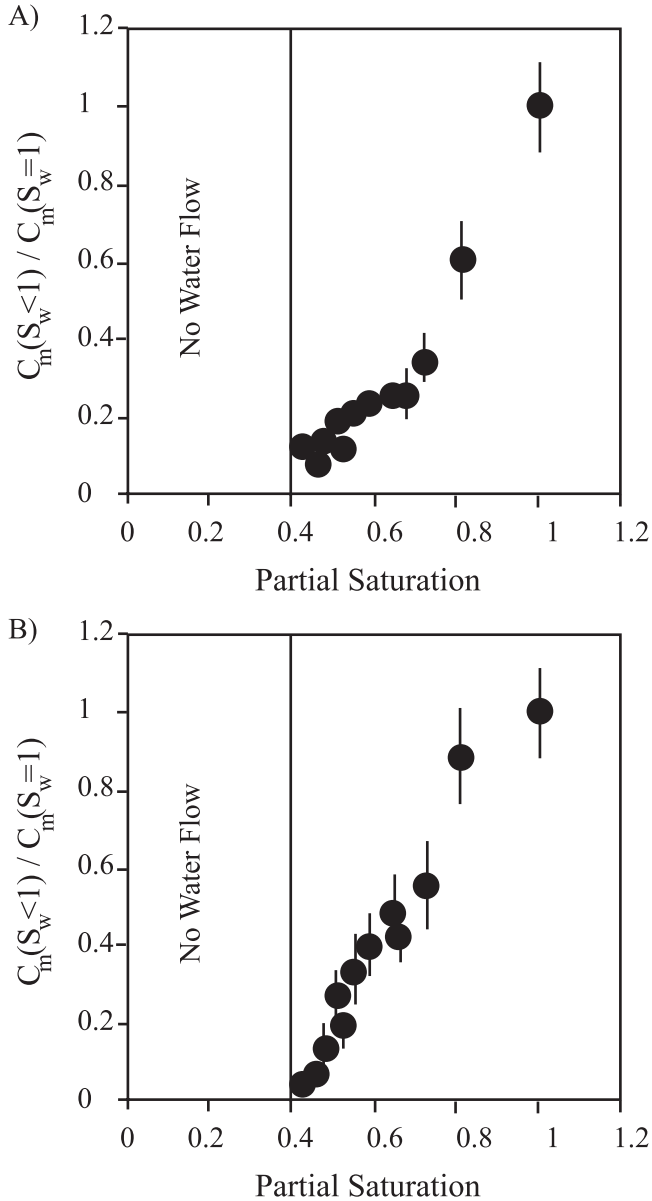

Figure 11. Normalized coupling coefficient $C_m(S_w < 1)$/$C_m(S_w = 1)$ versus water saturation. The ζ-potential is assumed to be insensitive to water saturation, and is calculated using equation (8). The gas injected is argon. (a) The experimental results are corrected for pH (equation (12)) and fluid electrical conductivity (equation (9)) variations in ζ-potential are corrected to a pH value of 8 and a fluid electrical conductivity value of of 140 μS/cm. (b) The experimental results are corrected for pH (equation (12)) and fluid electrical conductivity (equation (10)) variations in ζ-potential are corrected to a pH value of 8 and a fluid electrical conductivity of 140 μS/cm.

coupling coefficient decreases while the water saturation decreases, and equals zero as the water saturation reaches 40%. The behavior of the normalized coupling coefficient is not greatly affected by the ζ-potential changes versus water conductivity according to either equation (9) (Figure 11a) or equation (10) (Figure 11b). The normalized coupling coefficient is not in agreement with equation (11), but decreases according to a rough linear relation with water saturation. The phenomenological equation (8) does not take into account the water saturation S_{w0} under which the water in the porous media does not flow. According to Figure 11, the water saturation S_{w0} can be estimated to be about 40%. Note that when the water saturation is 40% (experiment 29 in Table 3), the water starts to flow out of the column 75 min after the beginning of the gas circulation. Our measurements in the case of argon can be explained by equation (8) if the water saturation is replaced by the effective water saturation. We do not observe any enhancement of the coupling coefficient with two-phase flow as reported by *Antraygues and Aubert* [1993] and *Sprunt et al.* [1994]. Nevertheless, the electrical resistivity of the porous medium increases by a factor of ∼5 when the water saturation ranges from 100 to 40% (Figure 4). During experiments, *Antraygues and Aubert* [1993] injected wet steam in a vertical column. Initially their medium was not saturated, and was at room temperature. The steam warmed and condensed into the column. The authors did not control humidity, and could not distinguish the effect of partial saturation from the effect of temperature. An increase of temperature enhances the ζ-potential, and therefore the coupling coefficient [*Ishido and Mizutani*, 1981]. *Sprunt et al.* [1994] performed experiments on limestone samples, in which they injected gas bubbles. They observed an increase of 2 orders of magnitude in the coupling coefficient in partial saturation. However, they did not use nonpolarising electrodes; futhermore the authors mentioned that gas bubbles were trapped in the electrode enclosures, and that the voltage was unstable during the passage of the bubbles. Therefore the increase of the coupling coefficient observed by *Sprunt et al.* [1994], was probably due to bubbles being trapped in the electrodes, which cannot occur in our experimental setup because porous ceramics were used.

[33] Finally if we assume that the water saturation S_{w0} is close to 40%, we can calculate the coupling coefficient in partial saturation conditions according to equation (3), for an effective saturation greater than the critical saturation S_e^c, which is in our case about 50%. In Figure 12, the calculated coupling coefficient, assuming a ζ-potential independent of water saturation (using equation (9)), is plotted versus the measured coupling coefficient. The calculated coupling coefficients are not in agreement with the measured ones.

[34] We carried out experiments with carbon dioxide to take into account chemical changes in two-phase flow conditions. When carbon dioxide is forced through the sand column, the pH of the solution ranges from 5.8 to 7.9, and the electrical conductivity of the solution ranges from 1.6×10^{-2} to 0.18 S/m. Carbon dioxide circulation leads to lower pH and higher electrical conductivity of the solution than argon and nitrogen circulation does, because carbon dioxide is a reagent gas at room pressure and temperature. When the electrical conductivity of the solution increases, the coupling coefficient decreases (equation 1). Thus for a given pressure difference, the induced voltages are smaller and their measurement is more difficult. The increase of 1 order of magnitude in the electrical conductivity of the solution

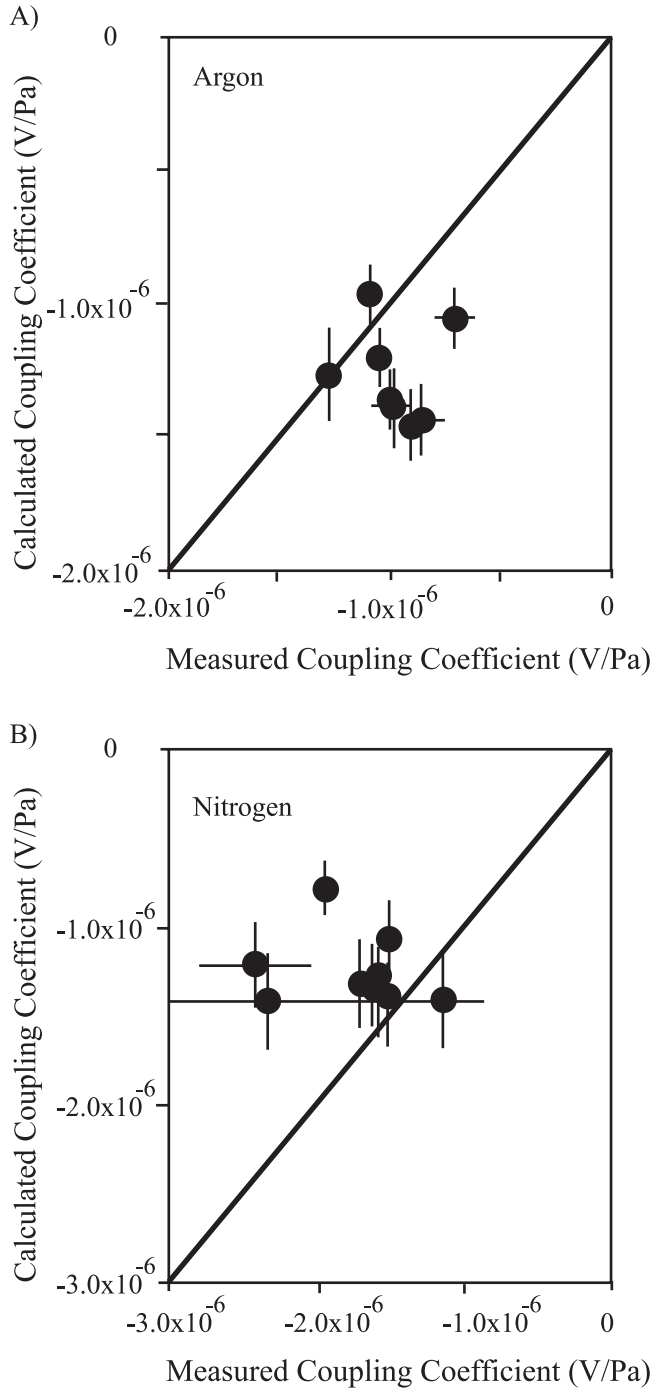

Figure 12. Coupling coefficient in partial saturation state. Comparison of the prediction of the coupling coefficient in equation (3) derived by *Revil et al.* [1999b] and our measurements, with the effective water saturation greater than the critical saturation S_e^c (about 50% for our sand). The ζ-potential is calculated according to equation (9). The line has a slope of unity to compare measured and calculated values. (a) Argon circulation. (b) Nitrogen circulation.

makes the determination of the coupling coefficient in saturated and in partially saturated state unreliable for the pressure differences that we can reach. Therefore we cannot deduce either an increase or a decrease of the electrokinetic coupling coefficient with decreasing saturation when carbon dioxide is used. However, if the electrokinetic coupling coefficient had been enhanced by a factor 10, we would have been able to measure it.

7. Conclusion

[35] The measured electrokinetic coupling coefficient in partial saturation is either constant or decreases by a factor of ~3 with decreasing water saturation from 100 to 40%, whereas the electrical resistivity is enhanced by a factor of ~5. Our measurements show that the critical saturation below which there is no longer fluid flow, and therefore no electrokinetic coupling, is about 40% for our sand. Our measurements are the first to provide the evolution of the coupling coefficient versus water saturation. Nevertheless we observe two different behaviors, so that it is not possible to provide a general evolution of the streaming potential in the partially saturated state. We hope that these measurements will motivate further theoretical and experimental investigations of electrokinetic phenomena in the partially saturated state.

[36] The main conclusion of our study for geophysical interpretation is that the electrokinetic coupling coefficient does not increase with decreasing water saturation. During laboratory measurements, the convection current due to fluid flow is exactly balanced by the conduction current. To interpret self potential measurements performed in the field, the convection current has to be calculated in partially saturated crust taking into account the increase of the electrical resistivity, but the electrokinetic coupling coefficient itself is not enhanced.

[37] **Acknowledgments.** We thank J.L. Thony and J.P. Laurent for providing us basic equipment of the sand column. We thank G. Marolleau for his help in the construction of the apparatus, N. Catel for water analysis, and L. Mamou for the X-ray diffraction analyses. This paper has been greatly improved by constructive remarks from the associated editor Kathy Whaler, the reviewer T. Ishido, and an anonymous reviewer. This research was supported by CNRS and by ACI Prévention des Catastrophes Naturelles. This is a CNRS-INSU-PNRH contribution 324 (thème circulation des fluides dans la croûte), and a CNRS-INSU-PNRN contribution 324 (Thème risques volcaniques).

References

Antraygues, P., and M. Aubert, Self potential generated by two phase flow in a porous medium: Experimental study and volcanological application, *J. Geophys. Res.*, *98*, 22,273–22,281, 1993.

Archie, G. E., The electrical resistivity Log as an aid in determining some reservoir characteristics, *Trans. Am. Inst. Min. Metall. Pet. Eng.*, *146*, 54–62, 1942.

Aubert, M., and G. Kieffer, Evolution d'une intrusion magmatique dans le flanc sud de l'Etna entre juin 1982 et juin 1983, Résultats de potentiel spontané (PS) et essai d'interprétation de l'éruption de 1983, *C. R. Acad. Sci., Ser. II*, *298*, 379–382, 1984.

Aubert, M., P. Antraygues, and E. Soler, Interprétation des mesures de polarisation spontanées (PS) en hydrogéologie des terrains volcaniques. Hypothèse sur l'existence d'écoulements préférentiels sur le flanc sud du Piton de la Fournaise (île de la Réunion), *Bull. Soc. Géol. France*, *164*, 17–25, 1993.

Beamish, D., Characteristics of near-surface electrokinetic coupling, *Geophys. J. Int.*, *132*, 231–242, 1999.

Bernard, P., Plausibility of long distance electrotelluric precursors to earthquakes, *J. Geophys. Res.*, *97*, 17,531–17,546, 1992.

Bussian, A. E., Electrical conductance in a porous medium, *Geophysics*, *48*(9), 1258–1268, 1983.

Davis, J. A., and D. B. Kent, Surface complexation modeling in aqueous geochemistry, in *Mineral Water Interface Geochemistry*, edited by M. F. Hochella and A. F. White, Mineral. Soc. of Am., Washington, D.C., 1990.

Dukhin, S. S., and B. V. Derjaguin, Electrokinetic phenomena, in *Surface and Colloid Science*, edited by E. Matijevic, chap. 1, pp. 1–48, John Wiley, New York, 1974.

Fenoglio, M. A., M. J. S. Johnston, and J. D. Byerlee, Magnetic and electric fields associated with changes in high pore pressure in fault zones: Application to the Loma Prieta ULF emissions, *J. Geophys. Res.*, *100*, 12,951–12,958, 1995.

Finizola, A., D. Ramos, and O. Macedo, Self potential studies of hydrothermal systems structure on Misti and Ubinas volcanoes south Peru, *XXIII Gen. Assem. EGS, Nice*, C194, 1998.

Finizola, A., F. Sortino, J. F. Lénat, and M. Valenza, Fluid circulation at Stromboli volcano from self-potential and CO_2 surveys, *J. Volcanol. Geotherm. Res.*, *116*, 1–18, 2002.

Garambois, S., and M. Dietrich, Seismoelectric wave conversions in porous media: Field measurements and transfer function analysis, *Geophysics*, *66*(5), 1417–1430, 2001.

Gibert, D., and M. Pessel, Identification of sources of potential fields with the continuous wavelet form: Application to self-potential profiles, *Geophys. Res. Lett.*, *28*, 1863–1866, 2001.

Glover, P. W. J., P. G. Meredith, P. R. Sammonds, and S. A. F. Murrell, Ionic surface electrical conductivity in sandstone, *J. Geophys. Res.*, *99*, 21,635–21,650, 1994.

Graciaa, A., G. Morel, P. Saulnier, J. Lachaise, and R. S. Schechter, The zeta-potential of gas bubbles, *J. Colloid Interface Sci.*, *172*, 131–136, 1995.

Ishido, T., and H. Mizutani, Experimental and theoretical basis of electrokinetic phenomena in rock-water systems and its applications to geophysics, *J. Geophys. Res.*, *86*, 1763–1775, 1981.

Ishido, T., and J. W. Pritchett, Numerical simulation of electrokinetic potentials associated with subsurface fluid flow, *J. Geophys. Res.*, *104*, 15,247–15,259, 1999.

Ishido, T., T. Kikuchi, N. Matsushima, Y. Yano, S. Nakao, M. Sugihara, T. Tosha, S. Takakura, and Y. Ogawa, Repeated self-potential of Izu-Oshima volcano, Japan, *J. Geomagn. Geoelectr.*, *49*, 1267–1278, 1997.

Jackson, D. B., and J. Kauahikaua, Regional self-potential anomalies at Kilauea volcano, *U.S. Geol. Surv. Prof. Pap.*, *1350*, 947–959, 1987.

Jiang, Y. G., F. K. Shan, H. M. Jin, L. W. Zhou, and P. Sheng, A method for measuring electrokinetic coefficients of porous media and its potential application in hydrocarbon exploration, *Geophys. Res. Lett.*, *25*, 1581–1584, 1998.

Jouniaux, L., and J.-P. Pozzi, Streaming potential and permeability on saturated sandstones under triaxial stress: Consequences for electrotelluric anomalies prior to earthquakes, *J. Geophys. Res.*, *100*, 10,197–10,209, 1995.

Jouniaux, L., and J.-P. Pozzi, Anomalous 0.1–0.5 Hz streaming potential measurements under geochemical changes: Consequences for electrotelluric precursors to earthquakes, *J. Geophys. Res.*, *102*, 15,335–15,343, 1997.

Jouniaux, L., S. Lallemant, and J.-P. Pozzi, Changes in the permeability, streaming potential and resistivity of a claystone from the Nankai prism under stress, *Geophys. Res. Lett.*, *21*, 149–152, 1994.

Jouniaux, L., M. L. Bernard, M. Zamora, and J. P. Pozzi, Streaming potential in volcanic rocks from Mount Pelée, *J. Geophys. Res.*, *105*, 8391–8401, 2000.

Lénat, J. F., D. Fitterman, and D. B. Jackson, Geoelectrical structure of the central zone of the Piton de la Forunaise volcano (Réunion), *Bull. Volcanol.*, *62*(2), 75–89, 2000.

Lorne, B., F. Perrier, and J.-P. Avouac, Streaming potential measurements, 1, Properties of the electrical double layer from crushed rock samples, *J. Geophys. Res.*, *104*, 17,857–17,877, 1999a.

Lorne, B., F. Perrier, and J.-P. Avouac, Streaming potential measurements, 2, Relationship between electrical and hydraulic flow patterns from rock samples during deformation, *J. Geophys. Res.*, *104*, 17,879–17,896, 1999b.

Malengreau, B., J. F. Lénat, and A. Bonneville, Cartographie and temporal observation of self-potential (SP) anomalies at Piton de la Fournaise, *Bull. Soc. Géol. France*, *165*, 221–232, 1994.

Malmberg, C. G., and A. A. Maryott, Dielectric constant of water from 0° to 100°C, *J. Res. Natl. Bur. Stand. U.S.*, *56*(1), 2641, 1956.

Park, S. K., M. J. S. Johnston, T. R. Madden, F. D. Morgan, and H. F. Morrison, Electromagnetic precursors to earthquakes in the ULF band: A review of observations and mechanisms, *Rev. Geophys.*, *31*, 117–132, 1993.

Pengra, D. B., S. Xi Li, and P. Wong, Determination of rock properties by low frequency AC electrokinetics, *J. Geophys. Res.*, *104*, 29,485–29,508, 1999.

Pride, S., Governing equations for the coupled electrmagnetics and acoustics of porous media, *Phys. Rev. B*, *50*, 15,678–15,696, 1994.

Pride, S., and F. D. Morgan, Electrokinetic dissipation induced by seismic waves, *Geophysics*, *56*(7), 914–925, 1991.

Revil, A., and P. W. J. Glover, Nature of surface electrical conductivity in natural sands, sandstones and clays, *Geophys. Res. Lett.*, *25*, 691–694, 1998.

Revil, A., P. A. Pezard, and P. W. J. Glover, Streaming potential in porous media, 1, Theory of the zeta potential, *J. Geophys. Res.*, *104*, 20,021–20,031, 1999a.

Revil, A., H. Schwaeger, I. L. M. Cathles, and P. D. Manhardt, Streaming potential in porous media, 2, Theory and application to geothermal systems, *J. Geophys. Res.*, *104*, 20,033–20,048, 1999b.

Roberts, J. J., and W. Lin, Electrical properties of partially saturated Topopah spring tuff: Water distribution as a function of saturation, *Water Resour. Res.*, *33*(4), 577–588, 1997.

Sailhac, P., and G. Marquis, Analytic potential for the forward and inverse modeling of SP anomalies caused by subsurface fluid flow, *Geophys. Res. Lett.*, *28*, 1851–1854, 2001.

Sigg, L., P. Behra, and W. Stumm, *Chimie des Milieux Aquatiques*, Dunod, Paris, 2000.

Sprunt, E. S., T. B. Mercer, and N. F. Djabbarah, Streaming potential from multiphase flow, *Geophysics*, *59*, 707–711, 1994.

Suman, R. J., and R. Knight, Effects of pore structure and wettability on the electrical resistivity of partially saturated rocks—A network study, *Geophysics*, *62*(4), 1151–1162, 1997.

Waxman, M. H., and L. J. M. Smits, Electrical conductivities in oil-bearing shaly sands, *Trans. AMIE*, *243*, 107–122, 1968.

Yoshida, S., Convection current generated prior to rupture in saturated rocks, *J. Geophys. Res.*, *106*, 2103–2120, 2001.

Zablocki, C. J., Streaming potentials resulting from the descent of meteoric water—A possible mechanism for Kilauean self potential anomalies, *Trans. Geotherm. Resour. Counc.*, *2*, 747–748, 1978.

Zlotnicki, J., M. Feuillard, and G. Hammouya, Water circulation on La Soufrière volcano inferred by self-potential surveys (Guadeloupe, Lesser Antilles). Renew of volcanic activity?, *J. Geomagn. Geoelectr.*, *46*, 797–813, 1994.

Zlotnicki, J., G. Boudon, J. P. Viodé, J. F. Delarue, A. Mille, and F. Bruère, Hydrothermal circulation beneath Mount Pelée inferred by self potential surveying. Structural and tectonic implications, *J. Volcanol. Geotherm. Res.*, *84*, 73–81, 1998.

Zohdy, A. A. R., L. A. Anderson, and L. J. P. Muffler, Resistivity, self-potential, and induced-polarization surveys of a vapor-dominated geothermal system, *Geophysics*, *38*(6), 1130–1144, 1973.

X. Guichet, L. Jouniaux, and J.-P. Pozzi, Laboratoire de Géologie and CNRS UMR 8538, École Normale Supérieure, 24 rue Lhomond, 75231 Paris Cedex 05, France. (xavier.guichet@ens.fr; jouniaux@geologie.ens.fr; pozzi@geologie.ens.fr)